Correction of finite spatial and temporal sampling effects in stereo-SCIDAR

Butterley, Timothy, Sarazin, Marc, Le Louarn, Miska, Osborn, James, Farley, Ollie J.

Timothy Butterley, Marc Sarazin, Miska Le Louarn, James Osborn, Ollie J. D. Farley, "Correction of finite spatial and temporal sampling effects in stereo-SCIDAR," Proc. SPIE 11448, Adaptive Optics Systems VII, 114481W (13 December 2020); doi: 10.1117/12.2562559

SPIE.

Event: SPIE Astronomical Telescopes + Instrumentation, 2020, Online Only

Correction of finite spatial and temporal sampling effects in Stereo-SCIDAR

Timothy Butterley[a], Marc Sarazin[b], Miska Le Louarn[b], James Osborn[a], and Ollie J.D. Farley[a]

[a]Centre for Advanced Instrumentation, Department of Physics, University of Durham, South Road, Durham, DH1 3LE, UK
[b]European Southern Observatory (ESO), Karl-Schwarzschild-Str. 2, D-85748 Garching, Germany

ABSTRACT

Stereo scintillation detection and ranging (S-SCIDAR) is a development of the well-established SCIDAR turbulence profiling technique. An S-SCIDAR instrument has been installed at the focus of one of the 1.8 m Auxiliary Telescopes at Paranal observatory since April 2016. We discuss the limitations imposed by the Paranal S-SCIDAR instrument's finite pixel size and exposure time. We present Monte Carlo simulation results quantifying the errors due to finite spatial and temporal sampling. We have reprocessed the existing S-SCIDAR dataset to compensate for these error sources; we discuss the impact of these corrections on the measured turbulence statistics.

Keywords: turbulence profiling, SCIDAR, atmospheric turbulence characterisation, dome seeing

1. INTRODUCTION

Stereo scintillation detection and ranging (S-SCIDAR)[1] is a development of the well-established SCIDAR[2] turbulence profiling technique. It observes the scintillation in the telescope pupil from two different stars on different detectors (rather than overlapping on the same detector), which yields improved sensitivity and allows a pair of stars with a larger magnitude difference to be used, thus increasing the number of available targets. It is a generalized SCIDAR,[3–5] meaning it is conjugated below the ground so as to make it sensitive to the ground layer.

The Paranal S-SCIDAR[6–8] was commissioned in 2016 on one of the 1.8 metre Auxiliary Telescopes (ATs). Since then it has accumulated a database of > 150 nights of turbulence profile with 250 m sampling. The design conjugation altitude of the instrument is -3 km, the pixel size is 1.8 cm and it operates with an exposure time of 2 ms.

This paper describes a number of systematic errors in the original S-SCIDAR pipeline that have been addressed in a new pipeline, and discusses the impact on turbulence statistics from the instrument. The paper is structured as follows: section 2 describes the aforementioned error sources. Section 3 compares the turbulence statistics from the dataset reprocessed with the new and old pipelines. Section 4 contains the conclusions.

2. ERROR SOURCES IN THE 2018A PIPELINE

This section describes a number of error sources that were present in the original SCIDAR turbulence profile fitting software that have been addressed in the new software. These errors affect data release 2018A.[8]

Further author information: (Send correspondence to T.B.)
T.B.: E-mail: timothy.butterley@durham.ac.uk, Telephone: +44 191 334 3714

Adaptive Optics Systems VII, edited by Laura Schreiber, Dirk Schmidt, Elise Vernet, Proc. of SPIE
Vol. 11448, 114481W · © 2020 SPIE · CCC code: 0277-786X/20/$21 · doi: 10.1117/12.2562559

2.1 Reference function scaling bug

Reference functions are the components of the model that are fitted to the SCIDAR cross-covariance to recover the turbulence profile. S-SCIDAR reference functions are generated via numerical integration of the formula[1,9]

$$B(r,h) = 0.078\pi k^2 C_n^2(h)\,\mathrm{d}h \int_0^\infty f^{-8/3} \sin^2(\pi\lambda h f^2) J_0(2\pi r f)\,\mathrm{d}f \tag{1}$$

where $k = 2\pi/\lambda$ and J_0 is a Bessel function of the first kind.

In the original pipeline, pre-calculated S-SCIDAR reference functions are used with a fixed turbulence strength of $C_n^2(h)\,\mathrm{d}h = 100 \times 10^{-15}$ m$^{1/3}$. Due to a bug in the code, these functions were not scaled correctly; they were a factor of 1.93 smaller than they should have been. As a result, all turbulence strengths were overestimated by a factor of 1.93. However, this overestimation was ameliorated somewhat by the other error sources discussed here.

2.2 Reference function sampling

The original S-SCIDAR pipeline took the point at the centre of a pixel as being representative of the whole pixel. For example, referring to figure 1, the covariance between the two shaded pixels was assumed to be given by the value of equation 1 for the distance between the two central crosses. This assumption is only sound in the regime where the scintillation-induced speckles are much larger than the pixels.

Ideally SCIDAR pixels should be small enough to sample the speckles well; 1 cm pixels are usually considered optimal.[10] In S-SCIDAR the pixels are larger than this, at 1.8 cm, so sampling the covariance only at the pixel centres is a poor approximation. In order to correct this, we need to calculate the covariance averaged over every point in the two shaded regions. This can be achieved by convolving the theoretical intensity covariance with the autocorrelation of a pixel mask function.

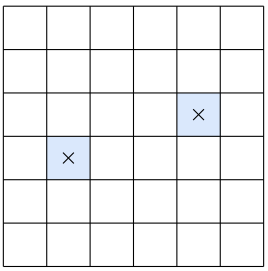

Figure 1. S-SCIDAR pixel sampling. Two sample pixels are shaded in blue, the centres which are marked with a cross.

Figure 2 shows examples of S-SCIDAR reference functions with this correction. Versions from theory and Monte Carlo simulation are both shown, and are in good agreement. The plots also show the unfiltered theoretical autocovariance (from equation 1) for comparison, and the reference functions from the old pipeline with the scaling error described in section 2.1.

Correlation peaks for shorter propagation distances are narrower, so are more strongly affected by poor sampling. The resulting error in the turbulence profile is therefore largest at the ground. The expected effect in the old pipeline due to this effect is an underestimation of the turbulence strength of $\sim 35\%$ for a propagation distance of 3 km, dropping off rapidly with altitude to $\sim 5\%$ for a propagation distance of 7 km (estimated from the relative heights of the theoretical autocovariance peak and the theoretical reference function peak in figure 2). Combined with the scaling error (section 2.1), this implies the old pipeline overestimated turbulence strength at all altitudes but by substantially more at higher altitudes than close to the ground.

Note that a Monte Carlo simulation must be sampled adequately in order to reproduce this effect. At first glance it may appear that it is sufficient to sample the phase and intensity field with the same sampling as the camera (i.e. 1.8 cm pixels). In fact the phase and intensity must be oversampled to model optical propagation

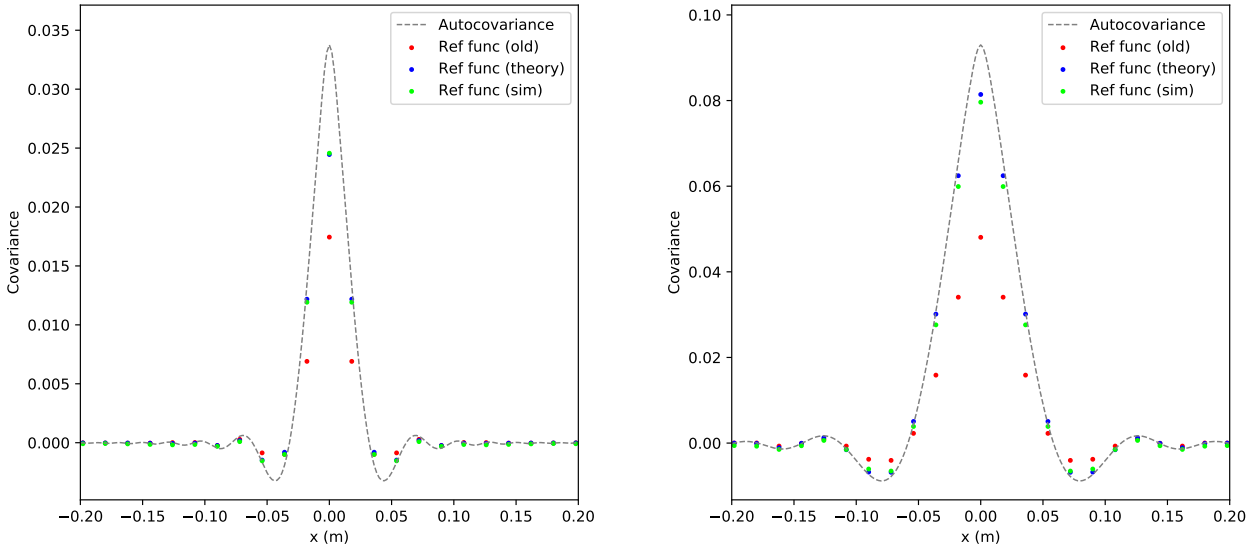

Figure 2. Example S-SCIDAR reference functions with 1.8 cm pixels for propagation distances of (left) 3 km and (right) 10 km.

through the atmosphere, and then the intensity field binned into detector pixels at the end (e.g. 4.5 mm sampling for the atmospheric propagation, binned 4×4 at the detector).

At the time of writing the authors have not found a detailed description of this correction in the literature. The error source is noted by Klückers et al[10] but they suggest calibrating against another instrument to correct it. Avila et al[11,12] mention taking into account spatial filtering of 2.8 cm pixels in a generalized SCIDAR experiment but no further details are provided.

2.3 Wind smearing

S-SCIDAR reference functions are generated using the assumption that the camera exposures (which are 2 ms long) are sufficiently short to freeze the scintillation pattern. If the wind speed of a turbulent layer is sufficiently high, the scintillation pattern generated by the layer will move and "smear" during the exposure[13]). The corresponding covariance peak will be elongated along the wind direction and will have a reduced peak value. Figures 3 and 4 show simulated covariance peaks illustrating this effect. For a given wind speed is it much more pronounced for low-altitude peaks but we generally expect lower wind speeds at lower altitudes. At higher (jet stream) altitudes the elongation is ameliorated by the much broader covariance peaks.

In order to quantify the effect of this smearing on profile recovery, the low-speed simulated covariance peak for a given altitude was fitted to the other peaks simulated at that altitude. The result is shown in figure 5. Wind smearing leads to an underestimation of the turbulence strength. A layer at 2 km with a speed of 10 m/s would be underestimated by ∼15%. A layer at 10 km with a speed of 30 m/s would be underestimated by ∼25%.

Note that here we are fitting an unelongated peak to a single elongated peak in isolation. In practice SCIDAR profile fitting involves fitting a row of adjacent peaks; if the elongation of the peak is aligned along the row then we would expect it to appear in the profile as a thick layer spanning multiple bins. In this case the integrated C_n^2 may be underestimated by a smaller amount (if at all).

The typical magnitude of the wind smearing error as a function of altitude can be estimated using ECMWF wind velocity profiles. Figure 6 shows the distribution of wind speed as a function of height according to ECMWF. By combining this wind speed distribution with the response plot (figure 5) we can construct figure 7,

Figure 3. Simulated S-SCIDAR covariance peaks for a single layer with propagation distances of (top to bottom) 3 km, 10 km, 20 km. At each height, from left to right, the peaks correspond to wind speeds: low (no smearing), 18 m/s, 36 m/s, 54 m/s, 72 m/s.

which shows the estimated distribution of response values as a function of altitude based on the wind speed distribution.

Figure 7 shows that underestimation of C_n^2 due to wind smearing is most severe in the $5-10$ km range, where the median underestimation is $10-20\%$. We expect layers around 8 km to be underestimated by $20-25\%$ a quarter of the time, and possibly by as much as $\sim 40\%$.

The wind smearing error could be compensated for a given turbulence profile if the simultaneous wind velocity profile was fully known; the error of each turbulent layer could then be estimated and corrected. However, obtaining a sufficiently accurate wind velocity profile is not trivial. ECMWF is a forecast rather than a measurement, and the wind velocity profile obtained by S-SCIDAR is incomplete (the velocity of every single layer is not necessarily recovered).

The solution adopted here is cruder but does not require any information about the wind velocity profile. Rather than fitting a single row of covariance peaks to the measured covariance map, a triple row of reference functions is fitted as illustrated in figure 8. The central row of reference functions fits the "unsmeared" component of the covariance peaks, and the additional reference functions fit the component that is smeared away from the axis by the wind.

It should be noted that this method of compensating for the wind smearing is not ideal; it is a partial correction that reduces the wind-smearing error in existing S-SCIDAR data where the exposure time is too long. The best solution to this problem is to use a sufficiently short exposure time to freeze the turbulence when acquiring the data.

2.4 Instrument conjugation

During testing of the new pipeline it was observed that the model being fitted to the cross-covariance was consistently a poor fit to the central region, corresponding to the ground layer, as shown in figure 9. The residual always contains a circular structure at the centre, indicating that the ground layer peak being fitted is not the correct shape.

This anomaly could possibly be explained by non-Kolmogorov turbulence in the dome. A brief exploration via Monte Carlo simulation suggested that this would require quite a dramatic change to the turbulence power

spectrum, for example reducing the exponent from 11/3 to much less than 3. This is not very consistent with the authors' previous experience of dome seeing.[14]

A more likely explanation is that the S-SCIDAR cameras are not conjugated to the intended altitude of −3 km, but rather some distance closer to the telescope pupil. The shorter propagation distance would imply a narrower covariance peak for the ground/dome layer, which is consistent with the data. The third panel in figure 9 shows (qualitatively) how the residual changes if the covariance maps are fitted assuming a conjugation altitude of −2 km; the structure observed at the ground is less pronounced i.e. the model is a better fit.

A shorter propagation distance would also imply that all of the measured scintillation is weaker than expected so the turbulence strength would be underestimated at all altitudes (but more so at the ground, where the relative change in the propagation distance is larger). It is therefore critically important to verify the conjugation altitude of the instrument. Doing so requires access to the instrument; this was planned for mid-2020 but was delayed due to the Covid-19 pandemic, so it is now expected to take place in early 2021.

3. STATISTICS OF REPROCESSED PROFILES

The existing Paranal S-SCIDAR data have been reprocessed using the new pipeline. Since the conjugation altitude of the instrument is in doubt, the data have been reprocessed multiple times assuming a range of values for the conjugation altitude. Here we concentrate on two possible conjugation altitudes: −3 km (the intended conjugation altitude of the instrument) and −2 km (chosen as a value that, roughly speaking, yields profiles that seem more consistent with the other available data).

Figure 10 shows the reprocessed and original median turbulence profiles (and quartiles) assuming conjugation altitudes of −3 km and −2 km. Note that the old pipeline results, shown for comparison on all of the following plots, always assume the conjugation altitude is −3 km. As expected, the ground layer strength is substantially higher if the assumed conjugation altitude is assumed to be −2 km.

Figures 11, 12 and 13 show histograms of r_0, θ_0 and τ_0 respectively. The histograms of r_0 are particularly interesting; r_0 seems unfeasibly low if the conjugation height is −3 km, but if it is −2 km there is quite good agreement with the values from the old pipeline.

Figure 14 shows histograms of the ground layer fraction below 575 m (GLF575). In this case, there is excellent agreement with the old distribution for the −3 km case, but the ground layer fraction is for the −2 km case. So depending on the conjugation height, either r_0 or GLF575 can agree with the old pipeline, but not both.

The median values of the atmospheric parameters plotted in figures 11–14 are summarised in table 1, and values for two further conjugation heights are included.

Table 1. Summary of median turbulence parameters from the original pipeline (assusming −3 km conjugation) and the new pipeline for a range of possible conjugation heights.

Parameter	Original	−3 km	−2.5 km	−2 km	−1.5 km
r_0 (m)	0.141	0.194	0.171	0.147	0.120
θ_0 (arcsec)	1.627	2.215	2.112	2.037	1.970
τ_0 (s)	3.219	4.328	3.975	3.663	3.359
$\bar{h}$ (km)	5.802	5.852	5.386	4.814	4.012
$\bar{v}$ (m/s)	13.447	13.832	13.229	12.462	11.076
GLF575	0.422	0.420	0.472	0.531	0.624

4. CONCLUSIONS

A new S-SCIDAR pipeline has been developed that addresses several error sources in the original pipeline. These include a scaling error of ~ 1.9 and the effects of finite pixel size and wind smearing. There is evidence to suggest that the Paranal S-SCIDAR instrument may not be conjugated to −3 km as intended, but may be closer to

the telescope pupil (e.g. around −2 km). The conjugation height will be verified in early 2021. In the mean time, the existing data have been reprocessed to produce turbulence profiles and statistics assuming a range of different conjugation altitudes.

ACKNOWLEDGMENTS

This study was funded by the European Southern Observatory (ESO).

REFERENCES

[1] Shepherd, H. W., Osborn, J., Wilson, R. W., Butterley, T., Avila, R., Dhillon, V. S., and Morris, T. J., "Stereo-SCIDAR: optical turbulence profiling with high sensitivity using a modified SCIDAR instrument," MNRAS **437**, 3568–3577 (Feb 2014).

[2] Vernin, J. and Roddier, F., "Experimental determination of two-dimensional spatiotemporal power spectra of stellar light scintillation. Evidence for a multilayer structure of the air turbulence in the upper troposphere.," *Journal of the Optical Society of America (1917-1983)* **63**, 270–273 (Jan 1973).

[3] Fuchs, A., Tallon, M., and Vernin, J., "Folding-up of the vertical atmospheric turbulence profile using an optical technique of movable observing plane," in [*Atmospheric Propagation and Remote Sensing III*], Flood, W. A. and Miller, W. B., eds., *Society of Photo-Optical Instrumentation Engineers (SPIE) Conference Series* **2222**, 682–692 (June 1994).

[4] Avila, R., Vernin, J., and Masciadri, E., "Whole atmospheric-turbulence profiling with generalized SCIDAR," *Applied Optics* **36**(30), 7898–7905 (1997).

[5] Fuchs, A., Tallon, M., and Vernin, J., "Focusing on a Turbulent Layer: Principle of the "Generalized SCIDAR"," PASP **110**, 86–91 (Jan. 1998).

[6] Wilson, R. W., "Stereo-SCIDAR Design Report (ESO-234072)," tech. rep., ESO Internal (2015).

[7] Wilson, R. W. and Osborn, J., "Stereo-SCIDAR Compliance Matrix (ESO-284093)," tech. rep., ESO Internal (2015).

[8] Osborn, J., Wilson, R. W., Sarazin, M., Butterley, T., Chacón, A., Derie, F., Farley, O. J. D., Haubois, X., Laidlaw, D., Le Louarn, M., Masciadri, E., Milli, J., Navarrete, J., and Townson, M. J., "Optical turbulence profiling with Stereo-SCIDAR for VLT and ELT," MNRAS **478**, 825–834 (2018).

[9] Roddier, F., "The effects of atmospheric turbulence in optical astronomy," *Progess in Optics* **19**, 281–376 (Jan. 1981).

[10] Klückers, V., Wooder, N., Nicholls, T., Adcock, M., Munro, I., and Dainty, J., "Profiling of atmospheric turbulence strength and velocity using a generalised SCIDAR technique," *Astronomy and Astrophysics Supplement Series* **130**(1), 141–155 (1998).

[11] Avila, R., Vernin, J., and Sánchez, L., "Atmospheric turbulence and wind profiles monitoring with generalized SCIDAR," *Astronomy & Astrophysics* **369**(1), 364–372 (2001).

[12] Avila, R., Carrasco, E., Ibanez, F., Vernin, J., Prieur, J.-L., and Cruz, D., "Generalized SCIDAR Measurements at San Pedro Mártir. II. Wind Profile Statistics," *Publications of the Astronomical Society of the Pacific* **118**(841), 503 (2006).

[13] Caccia, J.-L. and Vernin, J., "Wind fluctuation measurements in the buoyancy range by stellar scintillation analysis," *Journal of Geophysical Research: Atmospheres* **95**(D9), 13683–13690 (1990).

[14] Butterley, T., Wilson, R. W., Sarazin, M., Dubbeldam, C. M., Osborn, J., and Clark, P., "Characterization of the ground layer of turbulence at Paranal using a robotic SLODAR system," MNRAS **492**, 934–949 (Feb 2020).

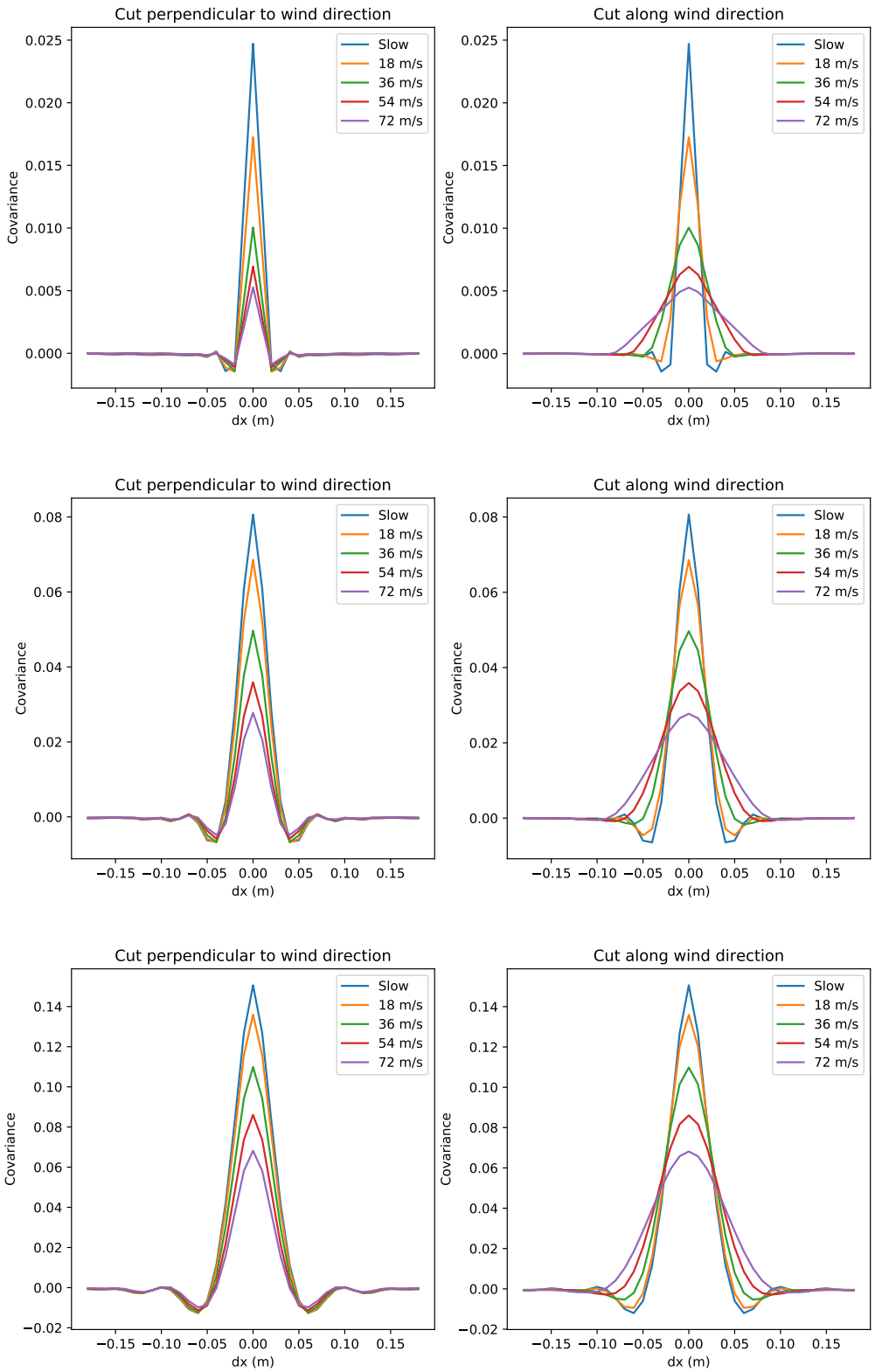

Figure 4. Cuts through simulated S-SCIDAR covariance peaks for a single layer with propagation distances of (top to bottom) 3 km, 10 km, 20 km.

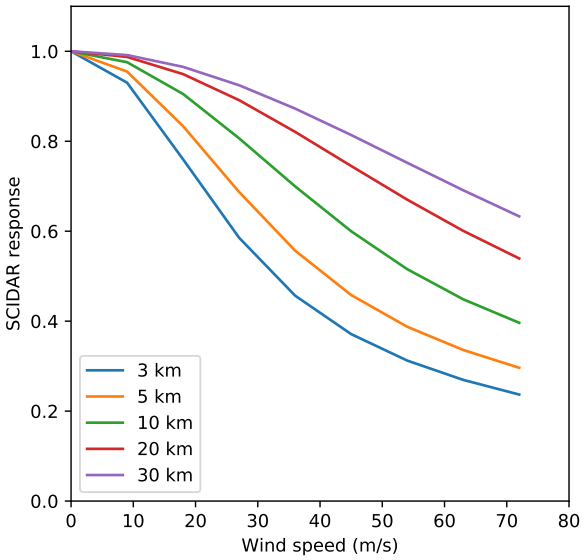

Figure 5. Plot showing response of S-SCIDAR to a layer with a given combination of wind speed and propagation distance.

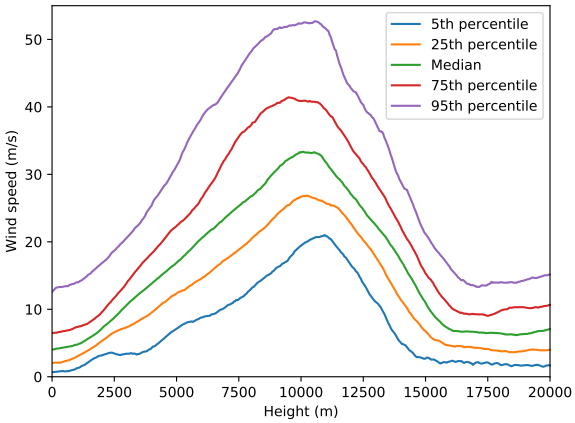

Figure 6. Wind profile distribution from ECMWF.

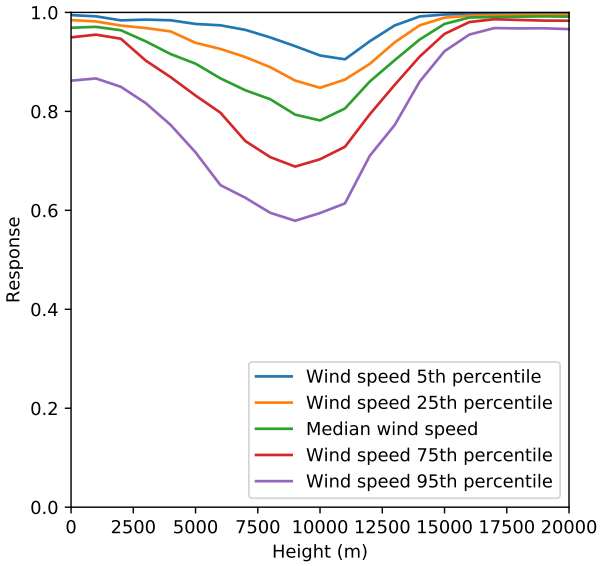

Figure 7. Plot showing range of reduction in S-SCIDAR response due to wind smearing as a function of altitude, based on the distribution of wind velocities from ECMWF data. Airmass 1.

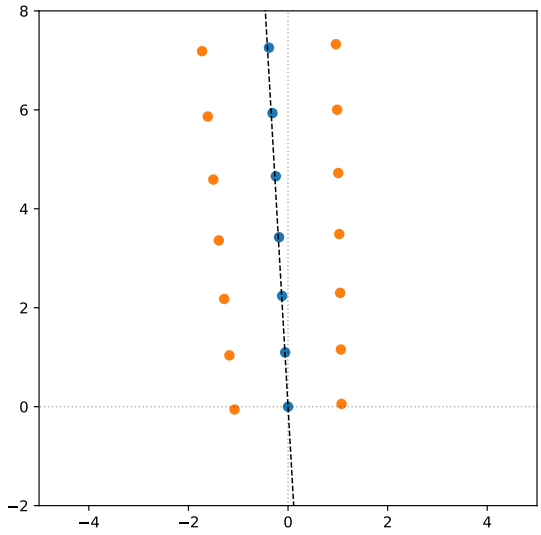

Figure 8. Locations of reference functions for profile recovery with wind smearing correction. Blue markers show the centres of standard reference functions. Orange markers show the centres of additional reference functions that serve to detect covariance that has been smeared away from the y-axis by high wind velocities. The black broken line shows the separation axis of the two stars (which is close to the y-axis but generally not perfectly aligned).

Figure 9. Left: central region of an example covariance map. Centre: corresponding region of residual map after fit assuming a conjugation height of −3 km. Right: corresponding region of residual map after fit assuming a conjugation height of −2 km. All 3 panels have the same colour scaling. The structures visible in the residuals are reduced significantly if the conjugation height is assumed to be −2 km rather than −3 km.

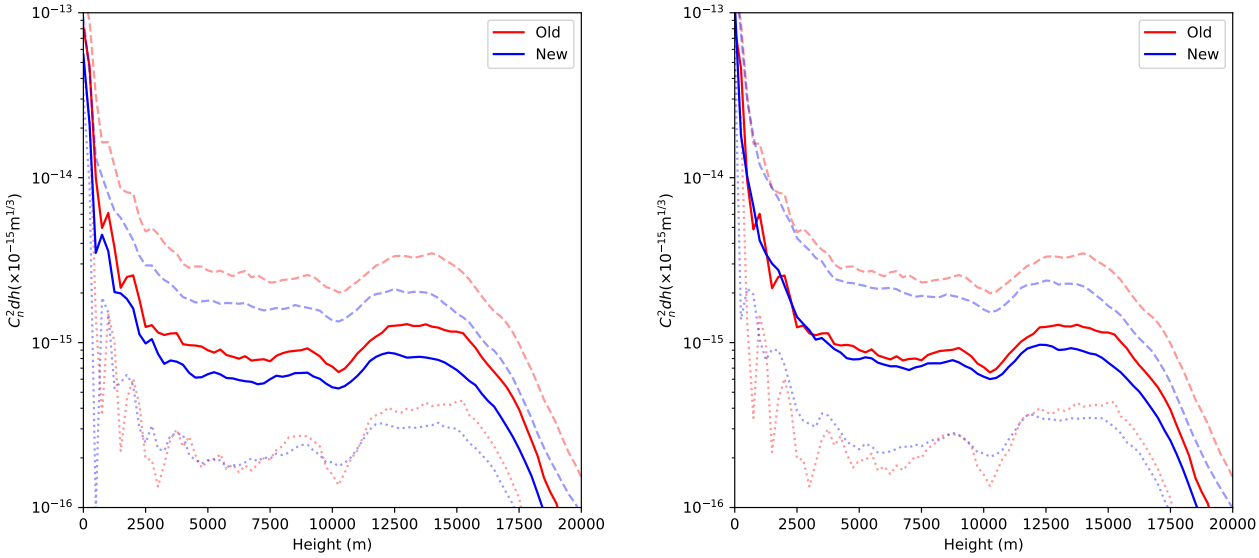

Figure 10. Median S-SCIDAR profiles (solid), 25th percentiles (dotted lines) and 75th percentiles (broken lines) for two possible conjugation heights. Left: −3 km, right: −2 km. The old profiles are shown in red (same in both plots).

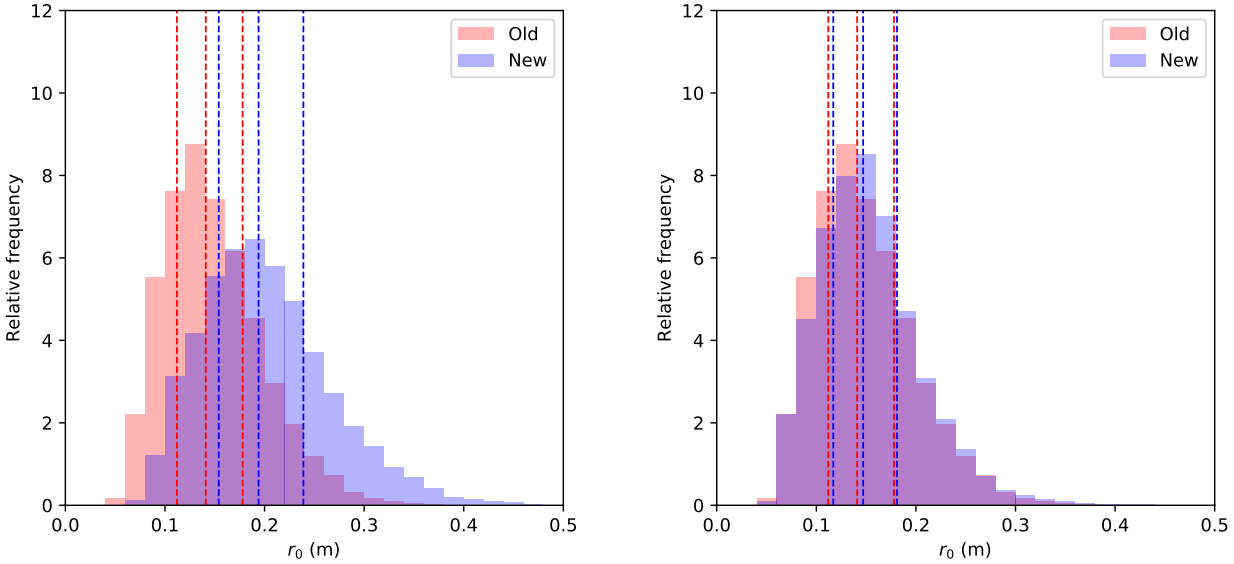

Figure 11. Histograms of S-SCIDAR r_0 for two possible conjugation heights. Left: -3 km (median 0.194 m), right: -2 km (median 0.147 m). The old (-3 km) case is shown in red (median 0.141 m).

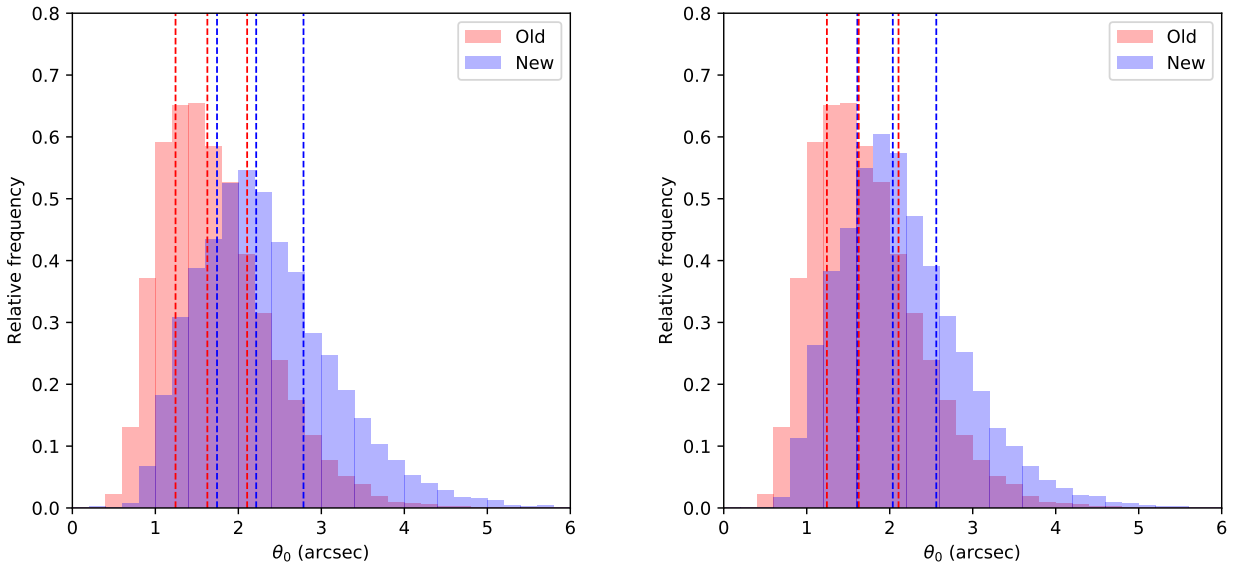

Figure 12. Histograms of S-SCIDAR θ_0 for two possible conjugation heights. Left: -3 km (median 2.22 arcsec), right: -2 km (median 2.04 arcsec). The old (-3 km) case is shown in red (median 1.63 arcsec).

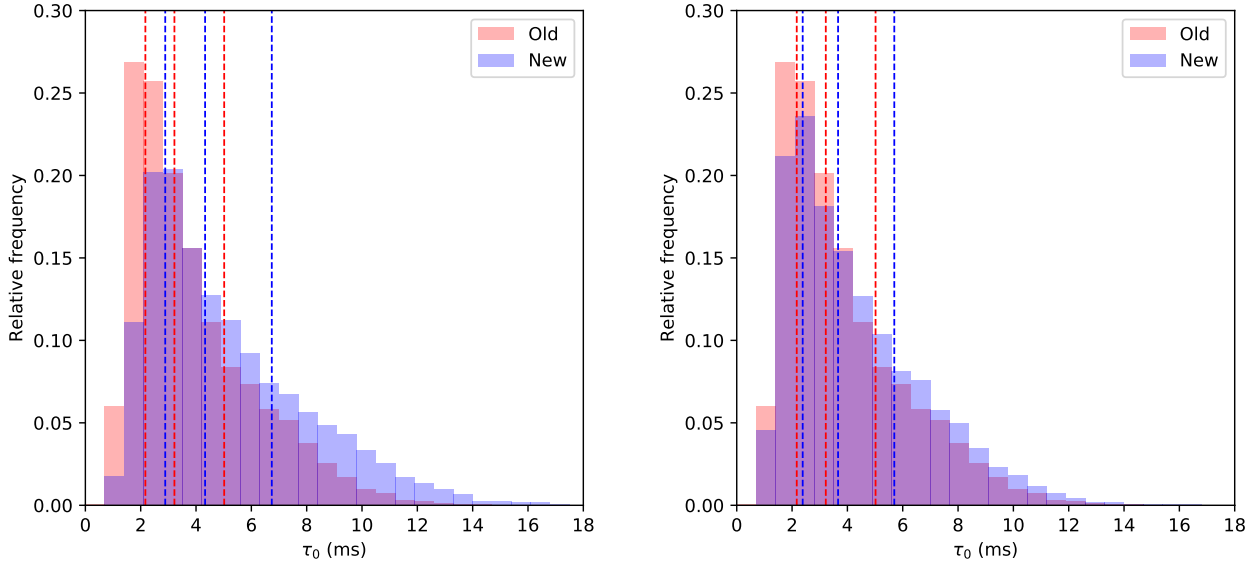

Figure 13. Histograms of S-SCIDAR τ_0 for two possible conjugation heights. Left: -3 km (median 4.33 s), right: -2 km (median 3.66 s). The old (-3 km) case is shown in red (median 3.22 s).

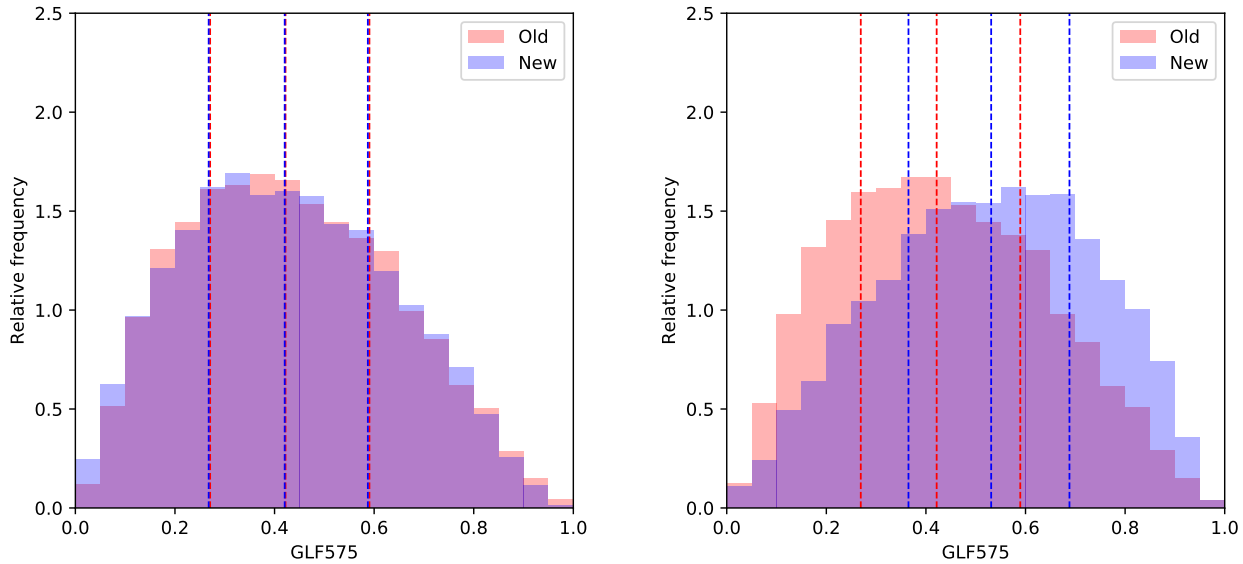

Figure 14. Histograms of S-SCIDAR ground layer fraction up to 575 m (GLF75) for two possible conjugation heights. Left: -3 km (median 0.42), right: -2 km (median 0.53). The old (3 km) cases are shown in red (median 0.42).